Relationship between local structures and ionic conductivity in Zr02-Y203 studied by site-selective spectroscopy

doi: 10.1103/PhysRevB.44.9214

PHYSICAL REVIEW B VOLUME 44, NUMBER 17 1 NOVEMBER 1991-I

Relationship between local structures and ionic conductivity in ZrO_2-Y_2O_3 studied by site-selective spectroscopy

H. Yugami, A. Koike, and M. Ishigame
Research Institute for Scientific Measurements, Tohoku University, Katahira 2-1, Sendai 980, Japan

T. Suemoto
The Institute for Solid State Physics, The University of Tokyo, Roppongi 7-22-1, Minato-ku, Tokyo 106, Japan
(Received 30 November 1990; revised manuscript received 9 April 1991)

The luminescence properties of Eu^{3+} ions in yttria-stabilized zirconia crystals are studied on samples with various yttria concentrations by using site-selective spectroscopy. From the analysis of luminescence spectra excited by ultraviolet light, it is found that the average crystal-field strength which acts on the Eu^{3+} ions increases with increasing dopant concentration. A detailed analysis of the site-selective spectra reveals that three distinct, but very similar sites for Eu^{3+} ions exist and, furthermore, the existence ratio of each site continuously changes with increasing dopant concentration. We propose local-structure models around the Eu^{3+} ions and discuss the relationship between local structures and ionic conductivity in this system.

I. INTRODUCTION

Yttria-stabilized zirconia (YSZ) is, at present, one of the most important and widely used oxygen-ion conductors in the high-temperature field.[1] Oxygen vacancies in YSZ are introduced by substitution of Y_2O_3 to preserve electrical neutrality. For Y_2O_3 concentrations between about 7 and 50 mol%, YSZ adopts the fluorite structure.[2] Since ionic conduction arises from oxygen-ion hoppings through anion-vacant sites, a monotonic increase of the ionic conductivity is expected with increasing Y_2O_3 concentration. However, the ionic conductivity exhibits a maximum at about 10 mol% Y_2O_3 and subsequently decreases with increasing Y_2O_3 concentration.[3]

The reason for this behavior of ionic conductivity has been investigated by many workers.[4–6] They have suggested that the decrease of conductivity may be attributed to the clustering or ordering of vacancies or second phase formation. Recently, studies of local structures in YSZ have been reported by using neutron[7] and electron-diffraction[8] techniques. Hull *et al.*[7] propose a model of local structure comprised of a vacancy-free tetragonal region and a region in which there are vacancies and aggregates of vacancy pairs. Suzuki *et al.*[8] state that the decrease of the ionic conductivity with increasing Y_2O_3 concentration can be attributed to an increase in the number of microdomains accompanying the Y_2O_3-type displacement of oxygen ions.

Spectroscopic studies of YSZ:L^{3+} systems have been reported by Arashi[9] and Dexpert-Ghys *et al.*[10] in connection with local structures in the systems, where L is a lanthanide. The latter authors measured luminescence spectra of Eu^{3+} ions in YSZ ceramics by using site-selective spectroscopy. They claimed that the observed site-selective spectra were the sum of luminescence from three different Eu^{3+}-ion sites, and assigned these three different sites to the Eu^{3+} centers having two oxygen vacancies, one oxygen vacancy and no oxygen vacancy at the nearest-neighbor oxygen sites. However, it seems that there is insufficient evidence to support the model of local structure proposed by these authors. Furthermore, there has never been any discussion about a quantitative evaluation of existence ratios of different sites as well as the relationship between the local structures and the ionic conductivity in this system.

In this paper, we try to understand the dopant concentration dependence of the ionic conductivity and the activation energy of ionic diffusion in connection with the interdefect interaction in this material, i.e., impurity-metal (M_{Zr}) –oxygen-vacancy (V_O), $M_{Zr}-M_{Zr}$, and V_O-V_O interactions. Furthermore, the difference in the dopant concentration dependence of ionic conductivity between YSZ and the Y^{3+}-doped CeO_2 system, which shows a maximum conductivity at about 4 mol% Y_2O_3, will be briefly mentioned in connection with the interdefect interactions in these systems.

For this purpose, we have made YSZ crystals comprised of optically active Eu^{3+} ions as a probe and investigated the local structure in the crystals by using site-selective spectroscopy.

Luminescence spectra of lattice disordered materials, such as superionic conductors, exhibit inhomogeneous broadening because of site-to-site variations in the local field which act on the ions. The technique of site-selective excitation provides a powerful tool for eliminating the inhomogeneous broadening from spectra and for obtaining detailed information on the local structure in disordered systems.[11] The Eu^{3+} ion is particularly well suited to such studies because of the simplicity of its energy levels and their sensitivity to the crystal-field environment. Furthermore, since the Eu^{3+} ions partially substituted the Y^{3+} ions, the local structure around the trivalent ions can be examined selectively by this technique.

II. EXPERIMENT

Transparent polycrystalline samples of YSZ:Eu^{3+} for several Y_2O_3 concentrations were grown by means of a xenon arc image furnace. They were cut and polished into rectangular shapes. By using the transparent samples, grain-boundary effects of samples on the luminescence spectra can be excluded and the intensity of the stray light scattered at the sample is drastically reduced compared with ceramic samples. In order to check the influence of the energy transfer between Eu^{3+} ions on the luminescence spectra, the concentration of the Eu^{3+} ion was varied from 0.01 to 1 mol % while the total concentration of L^{3+} ions was kept constant. No notable change was found at 15 K on the luminescence spectra measured on samples with different Eu^{3+} concentrations. Thus, we have used samples with 1 mol % Eu^{3+}-doped crystals in this study in order to obtain the spectra with high S/N ratio.

The samples were mounted into a closed-cycle He refrigerator and cooled down to 15 K. The excitation laser light was focused on the sample surface with a lens ($f=100$ mm) and fluorescence was collected and focused on an entrance slit of a monochromator by a camera lens ($f=50$ mm). Luminescence spectra under ultraviolet (uv) light excitation were obtained by using the 308-nm line of a XeCl excimer laser. For site-selective spectroscopy measurements, the excitation was provided by a pulsed dye laser (rhodamine 6G) pumped with the excimer laser. The tunable output of the spectral width of about 0.04 cm^{-1} was obtained in the 570-600-nm wavelength range. The luminescence is analyzed with a double monochromator (resolution limit of 2 cm^{-1}) equipped with a photomultiplier and a boxear integrator.

The luminescence intensity of the Eu^{3+} ion in YSZ was measured as a function of sample temperature. The intensity of luminescence was constant below room temperature and gradually decreased above that. The luminescence spectra disappeared above 400 °C.

Quenching effects on the luminescence spectra were also studied in this system in order to study the defect interaction between oxygen vacancies or between M_{Zr} and V_O at high temperature. YSZ exhibits the high ionic conductivity above 500 °C. Then, the starting temperatures for the quenching were set at 500, 1000, and 1400 °C. All samples were heated up to these temperatures for 3 h in air and subsequently quenched in water. Annealing of the quenched sample was performed at 1400 °C for 12 h in air.

III. RESULTS

Figure 1 shows luminescence spectra of Eu^{3+} ions excited by uv light in YSZ crystals with various dopant concentrations. These spectra correspond to the transitions between the $^5D_0$ and ^7F multiplets of Eu^{3+} ions. As seen in this figure, the luminescence bands of the transition from $^5D_0$ to $^7F_1$ Stark components seems to consist of three broad bands, i.e., all Stark components are split in this material. This result suggests that the local symmetry at the optical centers is much lower than that in the perfect fluorite structure, where the point-group symmetry at the metal ion is O_h. The broad spectra also suggest that there is a wide distribution of local field strength at the optical centers and, in consequence, the luminescence bands have a large inhomogeneous width. This result is in contrast to the situation in ordinary crystalline solids, where the bandwidth (inhomogeneous width) of the $^5D_0$-$^7F_0$ transition is very narrow, for example, about 1.7 cm^{-1} at 2 K in BaF_2:Sm^{2+}.[12] The homogeneous width of the $^5D_0$-$^7F_0$ transition of Eu^{3+} in YSZ is obtained by a fluorescence line-narrowing (FLN) technique and it is found that ratio of the inhomogeneous to the homogeneous linewidth is more than 10^3 at 15 K in this system. Results of the FLN measured on this system will be reported in a subsequent paper.

Another interesting feature of the $^5D_0$-$^7F_0$ band shown in Fig. 1 is the peak shift toward the higher-energy side with increasing the dopant concentration. This fact suggests that the average crystal-field strength which acts on the Eu^{3+} ions increases with increasing dopant concentration.

A series of site-selective spectra is obtained by tuning the dye laser light through the inhomogeneously broadened $^5D_0$-$^7F_0$ band of the Eu^{3+} ion. These spectra are presented in Figs. 2 and 3 for 9 and 19 mol % Y_2O_3-doped samples, which are represented by YSZ (9 mol %))

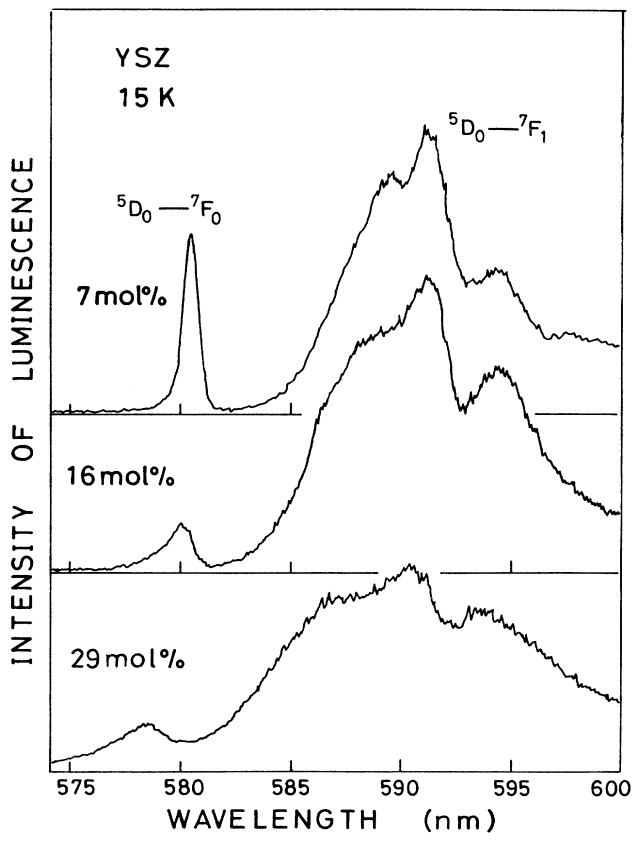

FIG. 1. Luminescence spectra of the Eu^{3+} ion in YSZ with 7-, 16-, and 29- mol % Y_2O_3-doped samples excited by uv-light.

and YSZ (19 mol %), respectively.

Since the luminescence bands in the site-selective spectra shown in Fig. 2 can be roughly decomposed into three broad bands, it is clear that the degeneracy of the $^7F_1$ state is completely removed in YSZ. This result suggests that the symmetry at the Eu^{3+}-ion sites in YSZ is C_{2v} or lower, in spite of the fact that the symmetry at the metal-ion site in the perfect fluorite structure is O_h.

Another salient feature of the site-selective spectra, notable in Fig. 3, is that the spectra of the $^5D_0$-$^7F_1$ region contain additional bands besides the three bands mentioned above. Thus, these bands are attributed to the luminescence of different sites with a different energy of the $^5D_0$-$^7F_1$ transition, which are simultaneously excited at one excitation wavelength.

In order to separate the spectra into components from different sites of the Eu^{3+} ion, the line shape of the luminescence band corresponding to the lowest Stark component observed in the wavelength region about 580–590 nm is carefully examined by changing the excitation wavelength because the line-narrowing effect is most significant for this component and its peak position is much more sensitive to the excitation wavelength than other peak positions. The peak position of luminescence bands are determined by the line-shape fitting using Gaussian curves. From this analysis, it is found that the lowest Stark component can be decomposed into three bands, which are labeled as "*A*," "*B*," and "*C*" in Fig. 3, and that the relative intensity among these bands changes by changing the excitation wavelength. We have assigned these three bands to the luminescence from Eu^{3+} ions at three different sites (*A*, *B*, and *C* sites).

It is also found from the line-shape fitting of all Stark components of the $^7F_1$ state that the $^7F_1$ state of Eu^{3+} ions in each site of *A*, *B*, and *C* fully splits into three Stark levels. This fact suggests that the point symmetry of all three Eu^{3+}-ion sites is C_{2v} or lower. The observed peak position of the luminescence bands in the $^5D_0$-$^7F_1$ region in YSZ (19 mol %) is plotted in Fig. 4 as a function of excitation wavelength. Although each of the luminescence bands related to the higher two Stark components can also be decomposed into three bands, the peak positions of these bands, especially weak intensity bands, cannot be uniquely determined by the fitting. So, the peak positions of the main bands observed at each excitation wavelength are plotted in Fig. 4 for the other two Stark components. As seen in Fig. 4, the splitting energy between the Stark components of the $^7F_1$ state of these three sites continuously increases with increasing excita-

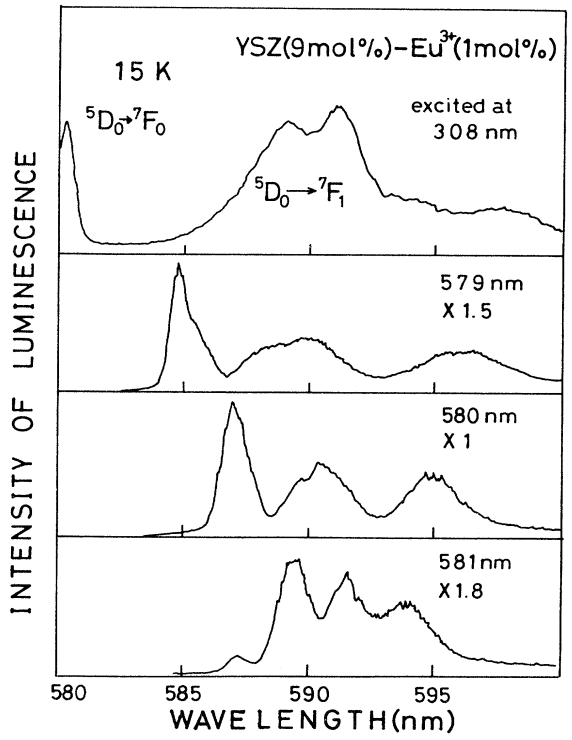

FIG. 2. Site-selective spectra of the Eu^{3+} ion in YSZ with 9-mol % Y_2O_3-doped samples excited by the dye laser light within the inhomogeneously broadened $^5D_0$-$^7F_0$ band, as shown in the top spectrum in this figure.

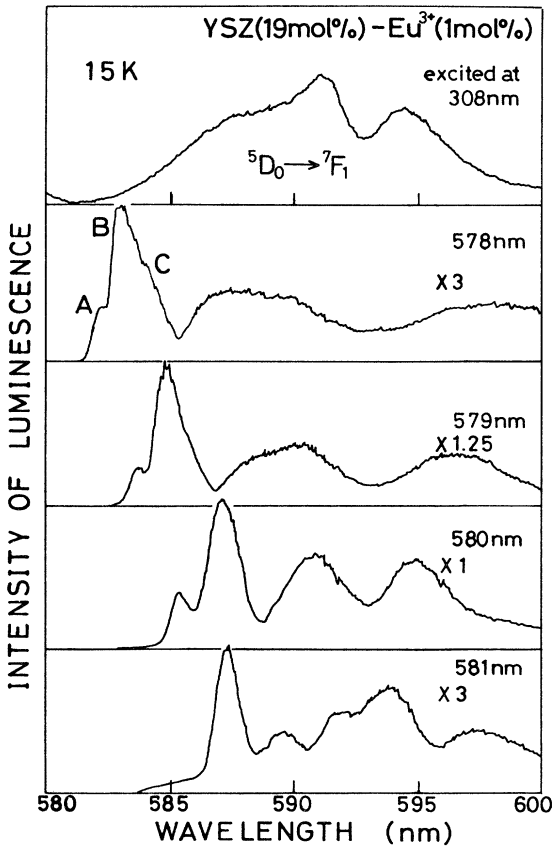

FIG. 3. Site-selective spectra of the Eu^{3+} ion in YSZ with 19-mol % Y_2O_3-doped samples excited by the dye laser light within the inhomogeneously broadened $^5D_0$-$^7F_0$ band, as shown in the top spectrum in this figure.

tion photon energy. This means that there are many different sites of Eu^{3+} ions which suffer slightly different crystal fields. This feature of the site-selective spectra is very similar to that observed in various glass materials.[13]

Although the line-narrowing effect is readily observed in the measured spectra, the linewidth of each band is far larger than the homogeneous width of the $^7F_1$ state of the Eu^{3+} ion [about 7 cm^{-1} at 300 K in $Ca(PO_3)_2$ glass[14]]. This fact means that inhomogeneous broadening remains in the site-selective spectra of YSZ. Such results often have been obtained from the site-selective spectra of the $^7F_1$ state of the Eu^{3+} ion under off-resonant excitation conditions (e.g., $^5D_0$-$^7F_0$ excitation).[15] The origin of the residual inhomogeneous linewidth may be due to accidental coincidence of excitation levels of ions in a different environment. Weber and Brawer have shown, by using a computer simulation technique, that the sites having approximately the same value of $^5D_0$-$^7F_0$ separation can have various values of splittings of the $^7F_1$ states.[16] From these results it can be concluded that the environment around Eu^{3+} ions in YSZ is quite similar with those in glass materials and, furthermore, the symmetry of all three Eu^{3+}-ion sites is much lower than that expected from the fluorite structure. This can be explained by considering the displacement of oxygen ions toward oxygen vacancies. Such a distortion of the oxygen sublattice has been observed in this material by several workers.[17–19]

IV. DISCUSSION

A. Dopant concentration dependence of local field strength surrounding impurity metals

The peak position and the bandwidth of luminescence of the $^5D_0$-$^7F_0$ transition are shown in Fig. 5(a) for samples with various dopant concentrations. With increasing dopant concentration, the peak position of the band shifts to higher energy and the bandwidth of this band considerably increases especially above 15 mol % Y_2O_3.

The dopant concentration dependence of the peak position and bandwidth of the $^5D_0$-$^7F_0$ fluorescence band indicates that the strength and the degree of fluctuations of the crystal field which acts on the Eu^{3+} ion increase with increasing dopant concentration. The following two reasons may be considered as origins of this result: (1) the increase of ionicity, or equivalently, the decrease of covalency, of bonds between the Eu^{3+} ion and ligand ions, and the (2) change of the average distance between the Eu^{3+} ion and ligand oxygen ions placed at the nearest-neighbor sites.

Systematic investigation of the relationship between the degree of covalency and the peak position of the $^5D_0$-$^7F_0$ band in various materials was reported by Caro *et al.*[20] They reported that a large degree of covalency of

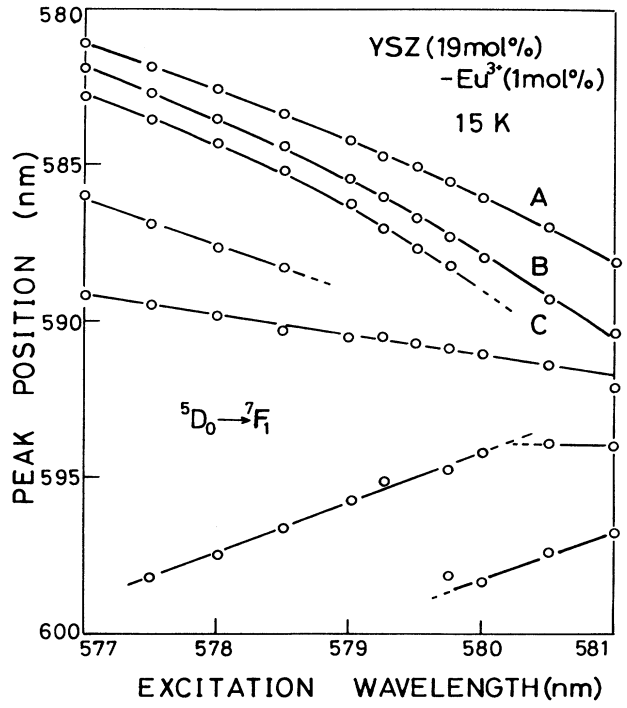

FIG. 4. The observed peak positions of several luminescence bands of the Eu^{3+} ion in YSZ (19 mol %) as a function of the excitation wavelength.

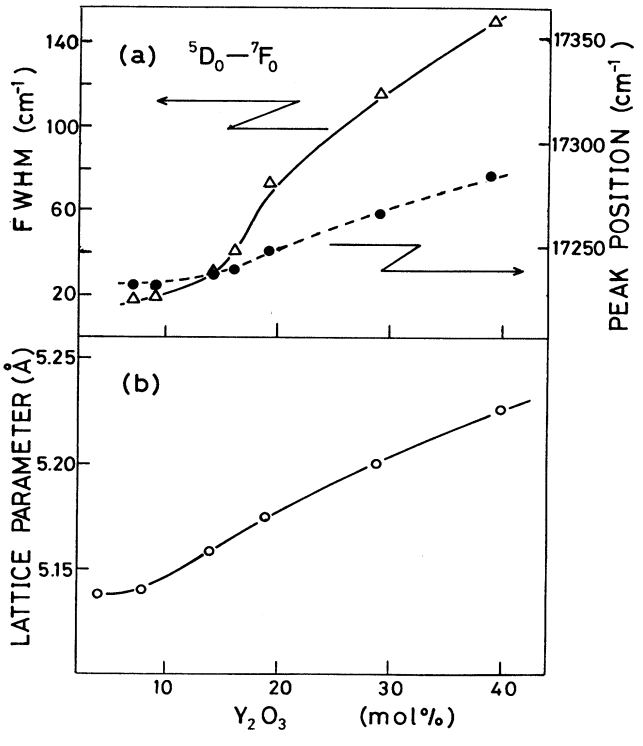

FIG. 5. (a) Dopant concentration dependence of the peak position and bandwidth of the $^5D_0$-$^7F_0$ transition of the Eu^{3+} ion. (b) Variation of the lattice constant of YSZ as a function of the dopant concentration.

bonds led to weaker Eu-ligand interactions producing a lower $^5D_0$-$^7F_0$ transition energy.

As it is well known, the ionicity of the bond is related to the effective charge Z in crystals and, in general, the increase of ionicity, equivalent decrease of covalency, leads to an increase of Z. The dopant concentration dependences of Z in YSZ have been measured by Ishigame *et al.*[21] with the infrared absorption technique. They found that Z decreased with increasing dopant concentration from the analysis of their results by using the virtual ion crystal model. They have concluded that the decrease of Z at high dopant samples is not due to the change of ionicity but the decrease of net charge in YSZ, which is caused by the substitution of Y^{3+} and the vacancy for Zr^{4+} and O^{2-} ions, respectively. Thus, their result rules out the possibility of case (1) for the origin of the stronger crystal field in high doped samples.

In case (2), shorter Eu ligand distance may lead to stronger interactions between them producing a higher energy of the $^5D_0$-$^7F_0$ transition. In most cases, the distance of Eu ligands is in proportion to the lattice parameter of the material, i.e., the large lattice parameter corresponds to the large distance of Eu ligands. The lattice parameter measured by the x-ray-diffraction method, which represents the mean distance between metal ions in this case, increases with increasing the dopant concentration as shown in Fig. 5(b). This result seems to rule out the possibility of case (2) for the origin of the stronger crystal field in high doped samples.

However, it must be considered here that the disorder of the oxygen sublattice exists in YSZ. The diplacement of oxygen and metal ions toward oxygen vacancies has been observed by several workers.[17,18,22] Steel and Fender[17] estimated the relaxation of oxygen ions toward a vacancy to be about 0.036 nm in YSZ (11 mol %). Veal *et al.*[22] state, on the basis of their results of the extended x-ray-absorption fine-structure (EXAFS) measurement, that the distance between metal and oxygen ions systematically decreases with increasing dopant concentration and, furthermore, the degree of fluctuation of the distance between them rapidly increases with increasing dopant concentration above 20 mol %. Using these results and the lattice parameter shown in Fig. 5(b), the decease of the Eu-oxygen distance is estimated to be about 10–15 % of the lattice parameter. The decrease of the distance between Eu and V_O is also estimated to be 10% of the lattice parameter. Taking these results into account, the increase of the magnitude of the local field strength at a high dopant concentration sample may be interpreted with the increase of the local fluctuation of the distance between the Eu^{3+} (or dopant) ion and oxygen ions, which will cause the wide distribution of the magnitude of the oxygen-ion displacement in the samples. In fact, it is clearly seen in Fig. 5(a) that the rapid upward shift of the peak position of the $^5D_0$-$^7F_0$ band corresponds well to the rapid increase of the bandwidth of the same band in the high doped region, especially above 15 mol %.

The above discussion should be related to the ionic transport property in this system. An increase of the interaction between a dopant ion and ligand oxygen ions, as well as oxygen vacancies, may lead to an increase of the binding energy between them. If a oxygen vacancy is trapped near a dopant ion site, it migrates by a hopping process. The activation energy of ionic diffusion, then, may be the sum of migration and association energies. In this condition, the increase of the binding energy between M_{Zr} and V_O will lead to an increase in the activation energy of ionic diffusion and, as a consequence, to a decrease in the ionic conductivity. Considering this effect on the ionic conduction process, it can be concluded that the very rapid increase of the activation energy of YSZ in the region from 15 to 20 mol % Y_2O_3 (Ref. 3) can be attributed to increase of the binding energy between the dopant metal and oxygen ion (or vacancy).

B. Dopant concentration dependence of local structures and interdefect interactions

In this section, we discuss the local structures of the different sites of Eu^{3+} and clarify the relationship between the ionic conductivity and the local structures. Three distinct Eu^{3+}-ion sites are found in the YSZ system by site-selective spectroscopy. It can be seen in Fig. 3 that the relative intensity of luminescence among these three sites changes with changing the excitation wavelength. The intensity and line shape of the luminescence band corresponding to the lowest Stark component, which can be decomposed into three (A, B, and C) bands as mentioned in Sec. III, are carefully examined by changing the excitation wavelength. The integrated area of each band of A, B, and C is considered to be the intensity of luminescence of the site at each excitation wavelength. The intensity of luminescence from the sites A, B, and C is plotted in Fig. 6 as a function of excitation wavelength. Three distinct profiles of the excitation spectra corresponding to A, B, and C are obviously observed for samples of YSZ (9 mol %) and YSZ (19 mol %). It is easily understood that the inhomogeneously broadened $^5D_0$-$^7F_0$ band is the sum of the contribution from the three different sites of Eu^{3+} ions. One salient feature of these excitation spectra is that the relative intensity of these bands changes with changing the dopant concentration.

In order to estimate the relative luminescence intensity of each site, the integrated are of the excitation spectrum shown in Fig. 6 is calculated for each site as the total intensity of luminescence from each of sites A, B, and C. In this procedure, the summation of each total area of the excitation spectra is normalized to unity in each sample. Using the relative intensity of luminescence among the sites of A, B, and C, we have estimated the apparent existence ratio of these three sites. Generally speaking, the relative luminescence intensity between different centers may not always be in proportion to the existence ratio of these centers because the quantum efficiency of luminescence of Eu^{3+} ions in each site may be different.[23] For this reason, we have estimated the quantum efficiency of luminescence from Eu^{3+} ions in each site. It is confirmed

from the result of the temperature and Eu^{3+} concentration dependences on luminescence spectra of YSZ:Eu^{3+}, both a nonradiative decay process and energy transfer process between Eu^{3+} ions do not contribute to the luminescence spectra measured at 15 K. Thus, we have estimated the quantum efficiency of luminescence from the radiative decay rate of each site. Using the estimated value of the quantum efficiency of the luminescence from Eu^{3+} ions, we calculate the net existence ratio of each site from the apparent existence ratio.

The dopant concentration dependence of $\rho(I)$, which is the net existence ratio of site I ($=A$, B, and C), is presented in Fig. 7. As seen in this figure, these three sites exhibit distinctive behavior with the variation of dopant concentration. $\rho(A)$ increases with increasing dopant concentration. In contrast to this, $\rho(B)$ decreases with increasing dopant concentration, and moreover, $\rho(C)$ is almost constant over the dopant concentration. These behaviors of $\rho(I)$ may be related to the change of the concentration of oxygen vacancies as well as that of the dopant metal ions. We consider that luminescence spectra may mainly be affected by the configuration of the nearest-neighbor (NN) ions, which are eight oxygen ions. Thus, we assume that the origin of the different dependence of dopant concentration of $\rho(A)$, $\rho(B)$, and $\rho(C)$ can be attributed to the difference of the number of oxygen vacancies placed at nearest-neighbor sites of the Eu^{3+} ions. Under this assumption, we will clarify the local structures of the sites A, B, and C.

Unfortunately, it is expected that the local symmetry at metal-ion sites in YSZ becomes much lower than those in a crystal having the ideal fluorite structure, even if oxygen vacancies do not exist at the NN oxygen sites of metal ions, because there is large distortion in the oxygen sublattice as mentioned the previous section. Thus, we cannot directly determine local structure models, in other words, the number of NN oxygen ions, from the number of the split $^7F_1$ Stark components. So, we have determined the local structure model of the three sites from the results of the dopant concentration dependence of $\rho(I)$ ($I=A$, B, and C) and the luminescence spectrum pattern of each site.

First, the excitation light is tuned in 581 nm, which is shown by an arrow in Fig. 6. Under this excitation condition, the luminescence from the Eu^{3+} ions of site A is

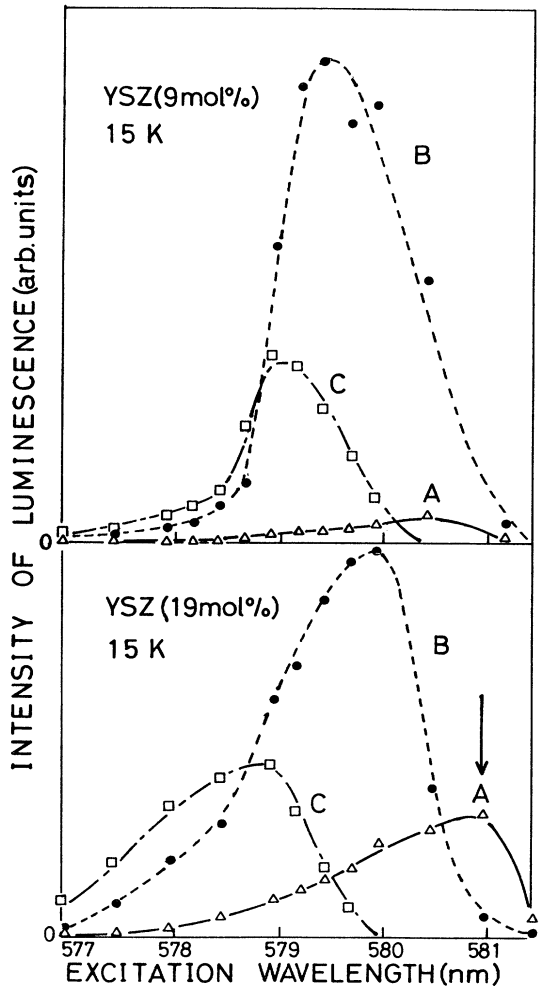

FIG. 6. Excitation spectra of the lower Stark component of the $^7F_1$ state in YSZ (9 mol %) and YSZ (19 mol %). The arrow shown in this figure indicates the excitation wavelength for the spectrum shown in Fig. 8.

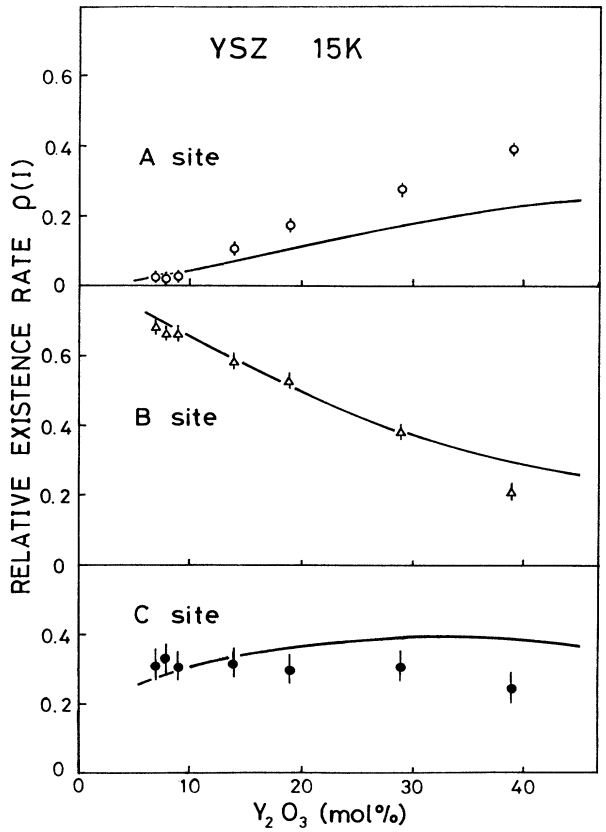

FIG. 7. Dopant concentration dependence of the relative existence ratio of sites A, B, and C in YSZ. The solid lines represent the calculated $\rho(I)$.

selectively excited. The luminescence spectra of the $^5D_0$-$^7F_{1,2}$ transition region of the Eu^{3+} ions in YSZ (19 mol %), as well as in Y_2O_3, are shown in Fig. 8. Making a comparison between these spectra, it is noticeable that most of the peak positions of all luminescence bands in YSZ (19 mol %) correspond well to those in Y_2O_3, while the bandwidth of the luminescence of YSZ (19 mol %) is much broader than that of Y_2O_3. This result strongly indicates that the local structure of site A in YSZ (19 mol %) may be very similar to that of the Eu^{3+} ions in Y_2O_3 and, then, the defect of the Y_2O_3-type structure may be created in YSZ system. This consideration is quite consistent with the dopant concentration of $\rho(A)$, which increases with increasing Y_2O_3 concentration.

The luminescence properties of the Y_2O_3:Eu^{3+} system were investigated by Dexpert-Ghys and Faucher.[24] The Y_2O_3 structure contains two different sites for the Y^{3+} ion, i.e., S_6 and C_2 sites. They assigned the observed luminescence spectrum of Eu^{3+} in Y_2O_3, which is almost the same one as shown in Fig. 8, to that from Eu^{3+} in the C_2 site. Considering this result, we assign site A to a local center accompanying two oxygen vacancies at face diagonal position in the NN oxygen-ion sites as shown in Fig. 9.

Second, site B is predominant in the region of lower dopant concentration and $\rho(B)$ decreases with increasing dopant concentration. From this result, it is natural to consider that the local structure of site B may relate to the fluorite structure, where no vacancy exists at the NN oxygen sites as shown in Fig. 9. Hull *et al.*[7] observed a region of vacancy-free tetragonally distorted fluorite structure by neutron scattering. This region observed by them may be related to the local structure of site B. However, since the luminescence of the $^7F_1$ state of Eu^{3+} at site B splits into three bands, the local symmetry at site B must be lower than tetragonal (T_d), where the three Stark components of the state must be all degenerate.

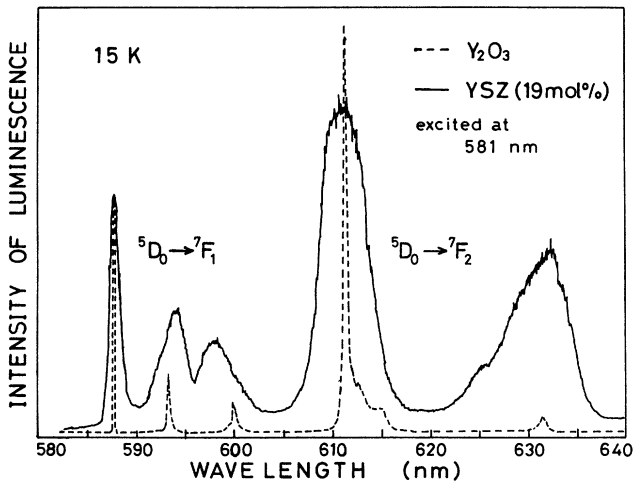

FIG. 8. Luminescence spectra of Eu^{3+} ions in YSZ (solid line) and Y_2O_3 (dashed line). Both spectra are excited at 581 nm.

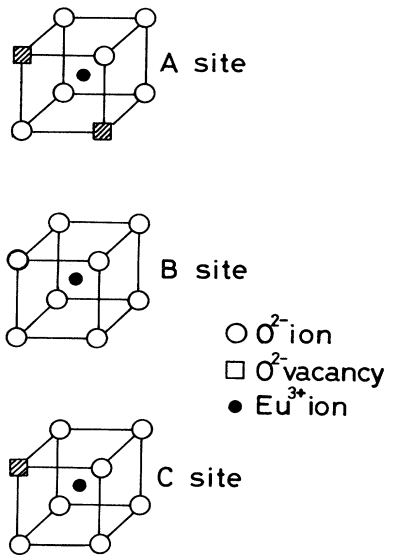

FIG. 9. Local-structure models for sites A, B, and C.

Finally, $\rho(C)$ is almost constant over the range of the dopant concentration. This indicates that site C exists constantly in YSZ and, then, the local structure of site C may have intermediate nature between the fluorite ZrO_2 and cubic-Y_2O_3 structures. For such a local structure, we consider a model for site C as shown in Fig. 9, where one vacancy exists in the NN oxygen-ion sites.

The local structure model shown in Fig. 9 is essentially the same as proposed by Dexpert-Ghys *et al.*[10] However, the site-selective spectra shown in their paper (Fig. 3 in Ref. 10) are measured on a highly doped sample [L^{3+}]=50 mol %) and are different from our results. Furthermore, the $^5D_0$-$^7F_1$ transition region in their luminescence spectra is not clearly observed by the influence of stray light scattered at the surface of ceramic samples. For these reasons, it is not clear whether our assignments of the relationship between observed luminescence bands and the three local structure models are the same as theirs or not.

To check the validity of the proposed model of local structures, the concentration dependence of $\rho(A)$, $\rho(B)$, and $\rho(C)$ were compared with those of calculated existence ratio of three sites. In this calculation, the interdefect interactions, i.e., V_O-V_O, M_{Zr}-V_O, and M_{Zr}-M_{Zr} are ignored. Under this assumption, the existence ratio of three sites is determined by the statistical distribution of vacancies and dopant ions. The concentration dependence of the calculated $\rho(I)$ is shown by solid lines in Fig. 7. In the region of lower dopant concentration below 10 mol %, agreement between calculated and experimentally estimated $\rho(I)$ is fairly good. Above 10 mol % dopant concentration, however, the calculated values deviate from the experimental value, and especially, $\rho(A)$ increases more rapidly than the calculated value. This disagreement may be related to the interdefect interac-

tion, which is neglected in the calculation. The rapid increase of $\rho(A)$ in the high dopant concentration region means that the interaction between oxygen vacancies becomes very strong in this region and it plays an important role for the formation of defect structures because site A consists of two oxygen vacancies at NN sites of the Eu^{3+} ion.

The dopant concentration dependence of the existence ratio and the strength of the intervacancy interaction can be related to the ionic conductivity of YSZ. The dopant concentration dependence of $\rho(A)$ shown in Fig. 7 suggests that the V_O-V_O interaction affects $\rho(A)$ in the region above 10 mol% Y_2O_3, and the interaction may be more significant for more than 20 mol% Y_2O_3-doped samples. In this high dopant concentration region, the decrease of the ionic conductivity has been observed in YSZ.[3] As described above, the local structure of site A is the Y_2O_3-type defect, which is considered as a vacancy-ordered structure where the vacancy cannot migrate as it does in the Y_2O_3 crystal.

From these considerations, the decrease of ionic conductivity as well as increase of activation energy of ionic diffusion in the higher dopant concentration region above 20 mol% may be attributed to the creation of the Y_2O_3-type defects (site A), in other words, to the creation of the vacancy-ordered clusters.

The creation of the structural modulation of the Y_2O_3 type has also been observed by the electron-diffraction measurement. Suzuki *et al.*[8] asserted that the increase of microdomains having Y_2O_3-type structure was responsible to the decrease of the ionic conductivity of YSZ. The conclusion obtained by this spectroscopic study is quite consistent with that obtained by Suzuki *et al.*

Another support for the validity of the model shown in Fig. 9 is obtained from the quenching experiment. Figure 10 shows the quenching temperature dependence of the relative intensity of luminescence of bands A, B, and C in YSZ (19 mol%) excited at 578 nm. In this figure, the total intensity of luminescence is normalized to unity in each sample. The luminescence intensity of bands A and B increases with increasing the quenching temperature T_q, especially $T_q > 1000$ °C. In contrast with these two bands, the intensity of the C band decreases with increasing T_q. These results indicate that the existence ratio among the A, B, and C sites is affected by the quenching process.

Since the mobility of metal ions is very small in YSZ below 1500 °C, the change of the local structure may be due to the structural change in the oxygen sublattice. Thus, we consider that the change of the relative luminescence intensity among three bands attributes to the change of the oxygen-vacancy configuration at the NN sites of Eu^{3+} ions. Under this consideration, we try to explain the result of the quenching experiment with a model shown in the inset of Fig. 10, which is based on the structural model shown in Fig. 9. With this model, one A and one B site are created from two C sites in the quenching condition and the inverse process takes place in the annealing condition (1400 °C, 12 h). Assuming the above processes, the variation of the relative luminescence intensity of sites B and C is calculated from that of site A (dashed line in Fig. 10). The result is shown in Fig. 10 with two solid lines. As seen in this figure, the calculated results agree well with the observed values. This result lends support to the local-structure model shown in Fig. 9.

Finally, we will compare the interdefect interactions in the YSZ system with that in the Y^{3+} doped CeO_2 system. Although both of these materials are typical oxygen-ion conductors having the same fluorite structure, the maximum conductivity is observed at about 10 mol% of dopant ion concentration in the YSZ system, while that is observed at about 4 mol% of dopant concentration in the Y^{3+}-doped CeO_2 system.

As discussed earlier in this paper, the relationship between the ionic conduction process and the interdefect interaction in YSZ is separately considered in the following two regions of dopant concentration. (1) In the region of 10–20 mol% Y_2O_3, the distance between M_{Zr} and V_O decreases with increasing dopant concentration which leads to the rapid increase of the strength of interaction between M_{Zr} and V_O. This, in turn, is responsible for the increase in the activation energy and equivalently, to the decrease of the ionic conductivity. (2) In the region above 20 mol% Y_2O_3, the interaction between V_O de-

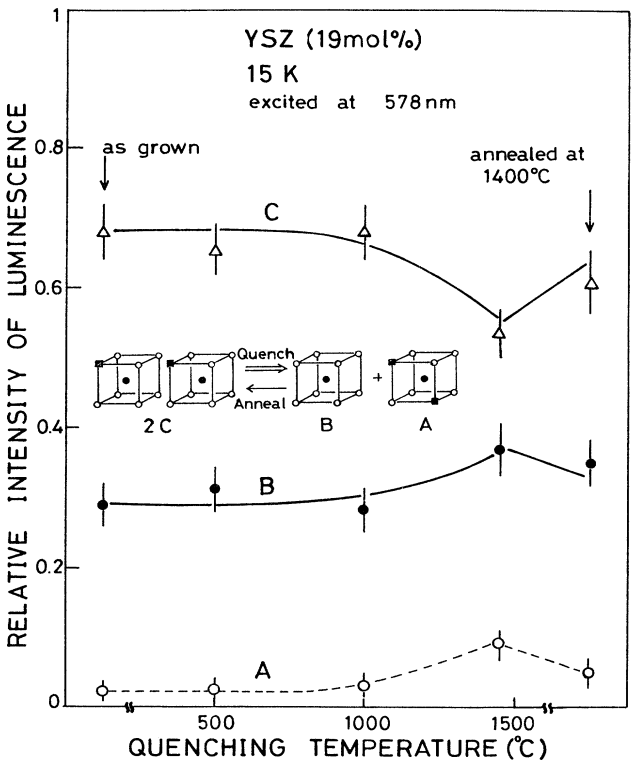

FIG. 10. Quenching temperature dependence of the relative intensity of luminescence among sites A, B, and C in YSZ (19 mol%) excited at 578 nm. The dashed line is drawn as a guide to the eye. The solid lines are calculated with a model shown in the inset (detailed discussion is given in the text).

fects, which lead to the creation of Y_2O_3-type defects, may be responsible for the increase of the activation energy.

On the other hand, in our previous study of the Y^{3+}-doped CeO_2 system,[25] it is revealed that the interdefect interaction between dopant metal ions and oxygen vacancies plays an important role for the ionic conduction process. Namely, it is found that the dopant concentration dependence of the ionic conductivity can be well interpreted by considering the interaction between the (V_O, M_{Ce}) defect and another M_{Ce} placed within the region of the fourth NN cation sites. In contrast with the case of YSZ, the following facts are found in the doped CeO_2 system: (1) the crystal field, which acts on Eu^{3+} ions, is almost constant over the dopant concentration region from 0.2 to 20 mol %, and (2) the interaction between oxygen vacancies does not play an important role for the ionic conducting process.

We consider that these differences of the interdefect interaction between the YSZ system and the Y^{3+} doped CeO_2 system are unambiguously responsible to the difference of the dopant concentration dependence of ionic conductivity in these systems. We now think that the origins of the difference of the interdefect interaction between them may be attributed to (1) the difference of the ionic radius between Zr^{4+} (0.072 nm) and Ce^{4+} (0.080 nm), and (2) the difference of the preferable coordination number (CN) between Zr^{4+} (a CN of 7) and Ce^{4+} (a CN of 8). Further study of the comparison of the ionic conducting processes between the above two systems is now being carried out in our laboratory by light scattering spectroscopy.

V. CONCLUSION

We have measured the luminescence spectra of Eu^{3+} in YSZ with various dopant concentrations. From the analysis of site-selective spectra, local structure models around Eu^{3+} ions are proposed. Experimental support for the model is obtained from both the dopant concentration and the quenching temperature dependences of the existence ratio among these sites. We have also discussed the relationship between the ionic conductivity and interionic interactions in this system. The dependence of the ionic conductivity in YSZ is well understood by considering the two different types of interdefect interactions. Namely, (1) in the region of 10–20 mol % Y_2O_3, the interaction between M_{Zr} and V_O may be mainly responsible for the increase of the activation energy and, equivalently, to the decrease of the ionic conductivity, and (2) in the region above 20 mol % Y_2O_3, the interaction between V_O defects, which lead to the creation of Y_2O_3-type defects, may be responsible for the increase of the activation energy. The difference of the dopant concentration dependence of ionic conductivity between YSZ and Y^{3+}-doped CeO_2 is unambiguously related to the difference of the interdefect interaction between them.

[1]W. L. Worrell, in *Solid Electrolytes,* edited by S. Geller (Springer-Verlag, Berlin, 1977), p. 143.
[2]P. Duwez, F. H. Brown, and F. Odell, J. Electrochem. Soc. **98**, (1951).
[3]D. W. Strickler and W. G. Carlson, J. Am. Ceram. Soc. **47**, 122 (1964); **48**, 288 (1965).
[4]M. Morinaga, J. B. Cohen, and J. Faber, Jr., Acta Crystallogr. A **36**, 520 (1980).
[5]A. G. Khachaturyan and B. I. Pokrovskii, Kristallografiya **25**, 599 (1980) [Sov. Phys. Crystallogr. **25**, 344 (1980)].
[6]C. R. A. Catlow, Solid State Ionics **12**, 67 (1984).
[7]S. Hull, T. W. D. Farley, M. A. Hackett, W. Hayes, R. Osborn, N. H. Andersen, K. Clausen, M. T. Hutchings, and W. G. Stirling, Solid State Ionics **28-30**, 488 (1988).
[8]S. Suzuki, M. Tanaka, and M. Ishigame, Jpn. J. Appl. Phys. **26**, 1983 (1987).
[9]H. Arashi, Phys. Status Solidi A **10**, 107 (1972).
[10]J. Dexpert-Ghys, M. Faucher, and P. Caro, J. Solid State Chem. **54**, 179 (1984).
[11]C. Brecher and L. A. Riseberg, Phys. Rev. B **13**, 81 (1976).
[12]R. M. Macfarlane and R. S. Meltzer, Opt. Commun. **52**, 320 (1985).
[13]J. Hegarty, W. M. Yen, and M. J. Weber, Phys. Rev. B **18**, 5816 (1978).
[14]E. Takushi and T. Kushida (unpublished).
[15]W. M. Yen and P. M. Selzer, in *Laser Spectroscopy of Solids,* edited by W. M. Yen and P. M. Selzer (Springer-Verlag, Berlin, 1981), p. 141.
[16]M. J. Weber and S. A. Brawer, J. Non-Cryst. Solids **52**, 321 (1982).
[17]D. Steele and B. E. F. Fender, J. Phys. C **7**, 1 (1974).
[18]J. Faber, Jr., M. H. Meuller, and B. R. Cooper, Phys. Rev. B **17**, 4884 (1978).
[19]D. W. Liu, C. H. Perry, A. A. Feinberg, and R. Currat, Phys. Rev. B **36**, 9212 (1987).
[20]P. Caro, O. Beaury, and E. Antic, J. Phys. (Paris) **37**, 671 (1976).
[21]M. Ishigame, E. Yoshida, S. Shin, and Y. Shimada, Solid State Ionics **20**, 105 (1986).
[22]B. W. Veal, A. G. McKale, A. P. Paulikas, S. J. Rothman, and L. J. Nowicki, Physica B **150**, 234 (1988).
[23]C. Brecher, L. A. Riseberg, and M. J. Weber, Phys. Rev. B **18**, 5799 (1978).
[24]J. Dexpert-Ghys and M. Faucher, Phys. Rev. B **20**, 10 (1979).
[25]H. Yugami, A. Nakajima, M. Ishigame, and T. Suemoto, Phys. Rev. B **44**, 4862 (1991).